# SYNTHESIS OF SMALL SILICON CARBIDE NANOCRYSTALS IN LOW PRESSURE NONTHERMAL PLASMA

A Thesis
Submitted to the Graduate Faculty
of the
North Dakota State University
of Agriculture and Applied Science

By

Reed Jeffrey Petersen

In Partial Fulfillment of the Requirements
for the Degree of
MASTER OF SCIENCE

Major Department:
Physics

April 2021

Fargo, North Dakota

# North Dakota State University
Graduate School

**Title**

SYNTHESIS OF SMALL SILICON CARBIDE NANOCRYSTALS IN LOW PRESSURE NONTHERMAL PLASMA

**By**

Reed Jeffrey Petersen

The Supervisory Committee certifies that this thesis complies with North Dakota State University's regulations and meets the accepted standards for the degree of

**MASTER OF SCIENCE**

SUPERVISORY COMMITTEE:

Prof. Erik Hobbie
Chair

Prof. Yongki Choi

Prof. Seth Rasmussen

Approved:

4/23/2021
Date

Prof. Sylvio May
Department Chair

# ABSTRACT

Nanoparticles have attracted much attention because of their unusual physical properties. This work represents original, incipient research into small crystalline silicon carbide nanoparticles synthesized in a low-pressure nonthermal plasma reactor. The nonthermal plasma technique offers a route for size-tunable synthesis of high-purity silicon carbide nanocrystals. Even though it has a high sublimation point, silicon carbide is synthesized in crystalline form in a nonthermal plasma reactor since nanoparticles are intensely heated by exothermic surface reactions on a nanoscale level. Using vaporized tetramethylsilane as a precursor and molecular hydrogen as an additive, both silicon carbide and silicon- or carbon-coated silicon carbide were created. Since plasma synthesis is a ligand-free process and charges on particles prevent agglomeration, silicon carbide is soluble in short-chain alcohols.

# ACKNOWLEDGMENTS

Many people have supported me academically and personally as I have pursued my master's degree in physics at North Dakota State University. I am grateful for all the assistance and support from the faculty and staff of the university through both my undergraduate and graduate degrees.

My deep thanks go to my adviser Dr. Erik Hobbie for his patience, encouragement, hard work, and extra time spent with me. He introduced me to the field of nanocrystal physics and has been a constant source of knowledge. His helpfulness as a teacher and mentor to me cannot be overstated, and I am grateful.

I also wish to acknowledge my lab coworkers, with whom I learned, brainstormed, and commiserated when the brainstormed ideas did not work as planned. Specifically, I thank Dr. Sam Brown for teaching me the ways of the glove box and confocal microscope. I thank Dr. Dr. Todd Pringle for his efforts in initial designs of the nonthermal plasma system at NDSU and for always being willing to stop by to talk for several hours when I had questions. Thanks to Salim Thomas for his support in the details of the nonthermal plasma system and for his friendship though my years researching. Thanks to Kenny Anderson for always being willing to answer questions on general and silicon-specific chemistries: Kenny's suggestions and ideas were invaluable to the effort. I would also like to thank Aaron Forde for his insightful conversations in the lab. In addition, I thank Dr. Jamie Froberg, Tim Twohig, Mahmud Sefanneser, and many more fellow researchers at NDSU who provided support and friendship.

I would like to thank co-authors whose help was without a doubt the driving force behind the research completed in my graduate years.

I wish to acknowledge and thank the stellar research group of Professor Amlan Pal at the Indian Association for the Cultivation of Science in Kolkata, India. Dr. Pal accepted me as a research student through the U.S. Fulbright program and accommodated me into his lab for a few months that went by too quickly, and I am very grateful. While there, I learned to make thin films and work with perovskite-hybrid materials from Soumyo da, Goutam da, Abhishek, and Subham, and my many other lab mates. I thank you all for introducing me to the culture, lab, and research community in Kolkata.

I would be remiss if I did not thank the outstanding "R2 Crew" who were helpful and accommodative when I needed to use the XRD at the last minute or squat in the thermal evaporator glove box for a few months. I specifically thank Greg Strommen for his assistance in equipping me to run various characterization equipment. I also thank Fred Haring for his help in procuring some apparatuses for our lab and Aaron Reinholz for administrative access.

My former advisers Dr. Sylvio May and Dr. Mila Kryjevskaia have also helped me greatly. I thank them for their guidance in nudging me toward the research track and on to pursue a master's degree.

# TABLE OF CONTENTS

# LIST OF FIGURES

# LIST OF ABBREVIATIONS

AC .....Alternating Current

DC .....Direct Current

DGU .....Density Gradient Ultracentrifugation

eV .....Electron Volt

IPA .....Isopropanol

LED .....Light Emitting Diode

MHz.....Megahertz

MFC .....Mass Flow Controller

NC .....Nanocrystal

NDSU .....North Dakota State University

NP.....Nanoparticle

PL .....Photoluminescence

RF .....Radio Frequency

SCCM.....Standard Cubic Centimeters per Minute

SiC.....Silicon Carbide

TEM .....Transmission Electron Microscopy

TGA.....Thermogravimetric Analysis

XRD .....X-Ray Diffraction

# INTRODUCTION

## Properties of silicon carbide

Silicon carbide (SiC) is a hard semiconductor material containing the elements of silicon and carbon in a 1:1 ratio. Because SiC can rarely be found in nature, it is typically made synthetically. SiC is chemically inert and does not oxidize until exposed to high temperatures. SiC does not melt at any known temperature.

The most common reason SiC is mass-produced is for its impressive mechanical properties. The right image in Figure 1 is carbide grit. SiC is used in many mechanical applications due to its extreme hardness. Some examples where silicon carbide is actively used are abrasives, high-performance ceramic car brake disks, and bulletproof plates. Fibers of SiC can be added in a polymer to form polymer matrixes with high strength-to-weight ratio.

Figure 1. Left side: A bulk single SiC crystal originally made by Texas Instruments that has yet to be sliced into SiC wafers. Right: Granular SiC 180-grit powder used as an abrasive. Images used with permission from eBay sellers lo-so59 and iain4670, respectively.

Bulk SiC has a density of 3.2 g/cm$^3$ at room temperature, which is very lightweight for its incredible yield strength of 21 GPa, and a bulk modulus of 220 GPa [1]. Accompanying its strength, SiC is brittle and hard, with the beta polytype having 95% of the hardness of diamond.

In its bulk crystalline form, SiC has a blueish-black or green color. SiC has a high thermal conductivity of 360 $W\ m^{-1}\ K^{-1}$ [1].

Because of its impressive mechanical properties, SiC became a popular material in the nineteenth century and was the subject of many scientific experiments. In the early 1900s, SiC's electrical properties were discovered, and it was used as a detector in the first radios. In 1907, Henry Joseph Round made the first light emitting diode (LED) by applying a voltage across a SiC crystal. The discovery of LED phenomena in SiC paved the way for large-scale production of green and blue LEDs.

SiC exists in over 250 crystalline polymorphs. The most common polytypes of SiC are 3C (cubic), 4H (hexagonal), and 6H. SiC in its 3C polytype has a band gap of about 2.36 eV, about twice that of silicon, and the hexagonal polytypes have a band gap over 3 eV. All of the polytypes of SiC are considered to be wide band gap. Optically, bulk SiC exhibits a low photoemission intensity at room temperature due to its indirect band gap [2].

Perhaps SiC's most desirable trait is its high electric field breakdown strength. Paired with its high maximum current density, these properties make SiC an attractive choice for high-powered devices. SiC can be doped using similar dopants to silicon. One application of bulk SiC at the forefront of technology is in the electric car, where intrinsic limitations of silicon are being reached due to battery and motor loads [3].

SiC is not the dominant technology in LEDs because its indirect band gap makes it less favorable for light emission than other materials, which have a higher brightness. Before the discovery of gallium nitride's usefulness in LEDs, 6H-SiC was used to make LEDs. Despite this, SiC is still used in LED production as it is a popular substrate for growing gallium nitride

devices (only a 3.4% lattice constant mismatch). Because of its heat dissipation characteristics, it is used as a heat sink in high-power LEDs.

Specific to physics, SiC can host quantum mechanical color centers, acting as a single-photon source. One notable point defect type is divacancy. The divacancy point defect in SiC has shown substantial coherence times of over 1.3 ms [4]. This has generated some interest for quantum computing applications.

SiC has traditionally been made for abrasives by combining silica sand and coke in a furnace at 2700 °C, which is crushed and size separated for different grits of abrasives. SiC is also produced on a small scale via thermal chemical vapor deposition by combusting trimethylsilyl chloride, at temperatures of about 1400 °C. SiC crystals have also been synthesized by supersaturation of carbon in a 1650-degree Celsius silicon melt [5].

**Properties of nanocrystals**

Nanoparticle (NP) research refers to an emerging field that includes synthesis and development of particles ranging in size from 1-100 nm, according to International Organization for Standardization and American Society for Testing and Materials standards [6, 7]. The momentum behind nanoparticle research is great, considering that a controlled method for the synthesis of nanocrystals was first developed in the 1990s by Moungi Bawendi [8], and it is now its own distinct field of research. Nanoparticles have many unique properties that lie between properties of bulk material structures and individual molecules. These properties commonly arise from a larger surface area to volume ratio, increased reactivity or stability in a chemical process, quantum confinement, enhanced mechanical strength, and other properties. Nanoparticles are unique from bulk materials because of their greatly increased surface area and small volume. Likewise, nanoparticles are unique from individual molecules because they can form lattices and

have group effects, such as semiconducting properties. Compounds consisting of carbon and hydrogen are organic compounds, but carbon compounds such as carbides are classified as inorganic. The inorganic core of NP is often arranged in a crystalline lattice structure, which would make the particle a subset of an NP, called a nanocrystal (NC). In this study, we will be investigating NC cores.

NPs can differ in various dimensions. They can be zero-dimensional when the length, width, and height of the particle are fixed to a dimension smaller than the nanoscale (for example, quantum dots), one-dimensional when two dimensions are confined to the nanoscale (such as nanowires), two-dimensional when one dimension is confined (such as thin films), or three-dimensional when all parameters are larger than the nanoscale. Sometimes this dimensional confinement can be on the same magnitude of the de Broglie wavelength of the electron wavefunction of the material. When materials become small enough to meet this condition, their electronic properties deviate significantly from bulk properties of the same material. If the particle exhibits photoluminescence (PL), quantum confinement will cause the emission wavelength of the particle to blueshift.

As the NPs have such a large surface area when compared to a similar mass of bulk material, the surface has a big effect on the behavior of the material. The surface can be uniform or irregular. Surface trap states are a complication for quantum dots due to their surface area, and the number of defects increases inversely to particle size [9, 10]. The surface can be charged also, which influences particle-particle interactions and particle-non-particle interactions, such as solubility. To passivate surface effects and defects, a core-shell structure is often adopted. Colloidal core/shell NPs contain at least two semiconductor materials in an onion-like structure. In such core/shell nanocrystals, the shell provides a physical barrier between the core, which

generally has the desirable electronic or luminescent properties, and the surrounding medium, thus making the NPs less sensitive to environmental changes, surface chemistry, and photo-oxidation. Ligands have the same effect of passivation and protection for the core of the NP. The surface of NPs can also be functionalized with molecules for many applications, including charge-transfer, biofluorescent labeling, and drug targeting.

**Synthesis of silicon carbide nanoparticles**

A wide variety of techniques have been used to synthesize SiC NPs. Broadly, synthesis routes of NPs can be broken down into two approaches: top-down and bottom-up approach. The top-down approach begins with the bulk material and uses various techniques such as grinding, etching, lithography, or implantation to reduce it down to NPs. The bottom-up approach begins with molecular precursors and builds the NP through nucleation or growth and can be performed through routes such as sol-gel synthesis or electrodeposition, or in plasmas. The bottom-up approach is typically favored for its efficiency and high-quality product. Due to SiC's high stability and tough mechanical properties, not all synthesis techniques for semiconductor NPs will work for SiC. Some techniques used for SiC synthesis are discussed below and broken down into two categories: non-plasma and plasma synthesis techniques.

**Non-plasma synthesis routes of silicon carbide nanoparticles**

The top-down approach is most common for SiC NPs. One prominent synthesis route is through carbothermic reduction of silicon, in which a carbon source and a silicon source are placed near to one another and heated for over six hours to several hundred °C under an inert atmosphere. After some lengthy post-processing to remove unwanted and unreacted precursors, the resultant is commonly 3C-SiC NC powder [11, 12, 13]. Most of the powder is sintered or heavily aggregated, which is a major disadvantage of this technique.

One form of commonly made SiC nanoparticle is in the form of one-dimensional whiskers. SiC whiskers are a single crystal fiber with a diameter in the nanometers and are used to enhance tensile strength and heat stability of composites. They are made by carbothermal reduction of silica ($SiO_2$) at 1400 °C [14]. Many times, the precursors for SiC NPs are natural materials such as agricultural waste [14] or recycled materials such as plastics [11], making them an attractive renewable process.

Another approach is based on electrochemical etching of bulk SiC. In this technique, a polycrystalline wafer of SiC is placed in a reservoir of the etchant — usually HF with another solvent such as ethanol — under current flow [15, 16, 17]. This etching creates a porous SiC matrix in the wafer, through which individual NCs can be liberated by sonication in a bath. This method is predictable because the structure of the SiC NCs will always take the same form as the parent wafer [17].

Yet another approach for the synthesis of SiC NCs is the sol-gel technique, which works for many of the group-IV semiconductor nanocrystals. This technique works in the following steps. First, a hydrolysis catalyst is added to certain types of polymeric carbon sources and heat is applied. When the polymer softens, a silicon precursor is added with water and a gel forms [18]. This gel is heated, and a vacuum is pulled to evaporate the water. Once it is heated to temperatures above 1000 °C, a carbothermal reaction takes place. This bottom-up approach is generally very high yield and produces dispersive particles. However, it is limited when compared to the other methods by the problem of incompatibility of the two precursors, which must be chosen carefully for the process to be successful [19].

Unfortunately, perhaps the biggest synthesis technique missing from SiC research, which many other semiconductor NPs have as an option, is liquid-phase colloidal synthesis. It is not

feasible for SiC because the precursors would have to be very unstable and highly exothermic to be able to form SiC. Thus, alternative synthesis techniques must be explored for SiC.

**Plasma synthesis of silicon carbide nanoparticles**

Notably, all bottom-up non-plasma synthesis techniques of SiC (whether bulk or nano-sized) requires exposure to high temperature, and the top-down approaches all require bulk SiC, which is made through high-temperature techniques. This high temperature is typically in a furnace or air-free chamber. High temperature ovens are costly (though cheap to run) and many purification steps have to be performed to obtain a relatively pure nanocrystalline product [20].

Plasma synthesis solves these problems because the resultant NCs are of pure form and the heat is localized to a smaller location (in nonthermal plasma synthesis, to the NC surfaces themselves), creating less waste heat.

One thermal plasma technique is laser pyrolysis, in which gaseous precursors — usually silane ($SiH_4$) and acetylene ($C_2H_2$) — absorb laser radiation, which directly dissociates the precursor molecules, and a nucleation and growth chemical process proceeds within a flame [21]. The flame has a temperature of above 1200 °C, and the species in the plasma are all at a similar temperature, making it a thermal plasma.

Another thermal plasma synthesis technique that has been used for SiC is the plasma expansion process. The experimental configuration consists of a DC plasma torch into which the precursors are fed (usually $SiH_4$ and $C_2H_2$), followed by a chamber for NP collection [22]. Generally, the DC plasma power source requires very high power to sustain the plasma (100+ amperes and 20+ volts), as the only plasma coupling is through the direct breakdown of the media (DC glow discharge) in a similar method to welding. While not all DC plasmas are

thermal, the plasma in the expansion synthesis process is thermal because of the morphological requirements of the reactor.

Finally, the technique used in this thesis is the nonthermal plasma process. This has been performed before by several research groups to achieve hollow crystalline SiC in low pressure plasmas [23], amorphous SiC NPs in low pressure plasmas [23, 24, 25, 26], and both amorphous and crystalline SiC NPs in atmospheric-pressure nonthermal plasmas [27]. Nonthermal plasmas are largely AC plasmas, and the coupling to the plasma of AC currents is either capacitive or inductive in nature, as opposed to the direct-breakdown coupling of thermal DC plasmas. The precursor chosen for this study is tetramethylsilane ($(CH_3)_4Si$ or TMS) because of its relatively low cost and ready availability. SiC NCs have never been made directly in a low-pressure nonthermal plasma, which is the motivation for this thesis.

**Introduction to nonthermal plasma**

Also called a cold plasma, nonthermal plasma derives its name from the fact that the electron temperature is much hotter than the temperature of the larger species in the plasma, such as silicon, carbon, or argon neutrals and ions. As only the electrons are the “hot” species, their velocity is much faster than the larger species and they have a hard time distributing their energy to their larger-species counterparts. This can be seen in Figure 2. An example of a common nonthermal plasma is found within a fluorescent lamp, in which a mercury-vapor gas is ionized. The electron temperatures reach 1-2 eV (up to 20,000 °C), while the rest of the gas remains slightly above room temperature, making it a safe household device (besides the mercury) [28].

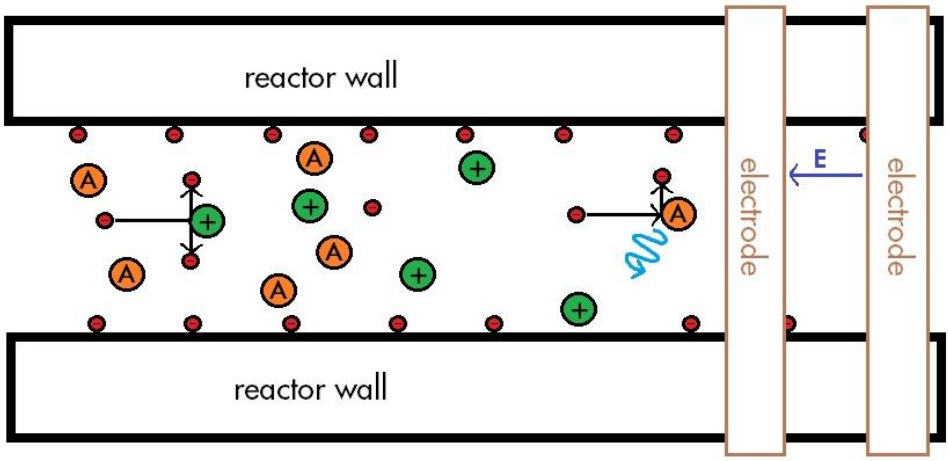


Figure 2. A schematic of the processes in a nonthermal plasma reactor. Adapted for the NDSU reactor from [29]. The right-most interaction depicts ionization of an atom, whereas the left interaction depicts an electron losing momentum and emitting a photon. A third common interaction exists, which is recombination of an electron and ion.

Nonthermal plasmas are efficient because there is little waste heat. When compared to NP synthesis by thermal DC plasmas, nonthermal radio frequency (RF) plasmas can be several orders of magnitude lower power. Our North Dakota State University (NDSU) reactor has made crystalline NPs from as little as 12 watts of net power put into the plasma. At such low powers, the reactor does not even require active cooling to remain operable. This efficiency is even more advantageous for making SiC because it is a high melting point material. SiC can be made directly in crystalline form since the nanoparticles are heated by surface reactions [30]. Surface reactions come about because of the electron collisions.

Electron population in plasmas is assumed to be Maxwellian, therefore we can use the Boltzmann equilibrium relation [29, 31, 32]:

$$n_{\phi_2} = n_{\phi_1} e^{-\frac{e(\phi_2-\phi_1)}{kT_e}} \quad \text{(Eq. 1)}$$

where $n_\phi$ is number density, $\phi$ is a local electrostatic potential, $k$ is the Boltzmann constant, and $T_e$ is the electron temperature. One important limiting case in this equation is that when the

electrostatic potentials are similar in value, the exponential term is near unity, which implies that the number densities will be similar.

Another delineation that exists between nonthermal plasmas is the pressure at which the plasma is operated. Input power required for breakdown of the plasma is directly proportional to the pressure of the plasma, thus atmospheric pressure plasmas will require much higher power densities to operate compared to low-pressure plasmas, which are on the order of magnitude of about 1 torr. With higher power densities come other practical concerns: active cooling has already been mentioned, but creating a reactor that can sustain the higher powers (as driving electrodes are traditionally external to the reactor, as depicted in Figure 2) is also important so that the electrodes do not physically etch the reactor. In atmospheric pressure plasmas, electrons have much shorter mean free path length, on the order of 1 micrometer. We chose a low-pressure plasma for the NDSU reactor, but this thesis investigates intermediary-pressure plasmas as well, with pressures in the tens and low hundreds of torr.

As with most synthetic, small-scale experimental plasmas, the quasi-neutrality condition holds true: if a gas of electrons and ions has a local non-zero net charge density, a strong electric field results which almost instantaneously neutralizes the net charge density. As a result of the ionic behavior of plasmas, long-distance electromagnetic forces create collective behaviors of ions, differing from neutral gases. This is broadly true within the plasma, with some notable exceptions. Larger elements in contact with the plasma, such as the reactor walls, will develop a net negative charge because the speed of the electrons in the plasma is much greater. This excess negative charge creates a sheath around the plasma, which confines the lower energy electrons to the body of the plasma, as in Figure 2.

NPs in a nonthermal plasma are mainly negatively charged, which prevents particle-particle agglomeration. This allows for the synthesis of ligand-free particles with very small diameters, between 1 and 10 nm. It is important to note that because walls of a nonthermal plasma reactor become negatively charged, the walls repel the NPs, which reduces losses of nanoparticles to the reactor wall in the area where there is active plasma.

**Applications of silicon carbide nanocrystals**

Nanosized SiC has a wider application field than bulk SiC. In addition to its bulk properties of high strength, corrosion stability, and semiconductor properties, SiC has interesting biological, sensor, and optical properties introduced at the nanoscale.

Nontoxicity makes them useful for biological applications, such as targeted biolabels and contrast agents. Encouraging results about the biocompatibility of SiC have come out in recent years [33]. 3C-SiC NCs have no significant cytotoxicity, making them a prospect for fluorescent probes in the human body to bridge the “green gap” for markers [34]. Nontoxicity in NCs is also important for the consumer, as it allows NC technology to be used in more home and child-safe products, and less worries about nanocrystals entering the water supply in low amounts.

Despite the potential benefits of using SiC NCs, their large-scale use seems distant in the future. Most of the scientific work on NCs is on group II-VI semiconductor materials. This has happened for two main reasons: the lack of understanding of the precise mechanism leading to emission in the visible range from SiC NCs, and the difficulty in synthesizing high purity SiC NCs. Group IV periodic element based NCs have an indirect band gap, so they have been largely passed over for efficiency optimized devices, such as LEDs and solar cells, in favor of direct band gap semiconductors. There have been some relatively efficient semiconductor NC devices made from group IV semiconductors [35, 36], but one promising new application for emissive

indirect band gap quantum dots is in luminescent solar concentrators which utilize the strengths of a large stokes shift [37].

SiC has been controversial in terms of its quantum confinement properties [38, 39, 40]. The Bohr radius of 3C-SiC is 2.0 nm [41, 42], 4H-SiC is 1.2 nm [41], and 6H-SiC is 0.7 nm [41, 42], having the implication that any material near or smaller in diameter than this value will exhibit quantum confinement effects due to electron confinement within the particle. In this size regime, surface effects also tend to have an increasing influence over the electronic properties of the NCs, which further clouds a clear interpretation of photonic and band gap characterization. PL has demonstrated conflicting results in the literature: many articles finding no PL at all. Absorption measurements are consistent however, with a rising edge in the near UV [38, 39].

# PRECURSOR CHOICE

The NDSU reactor detailed in the next chapter has been optimized for using liquid precursors. An ideal precursor is safe to work with, has a low toxicity, and should not be pyrophoric, as many low molecular weight silicon precursors are. The organosilicon compound tetramethylsilane fits these requirements well. Interestingly, this process transforms an organic precursor into an inorganic material. The structure of TMS can be seen in Figure 3.

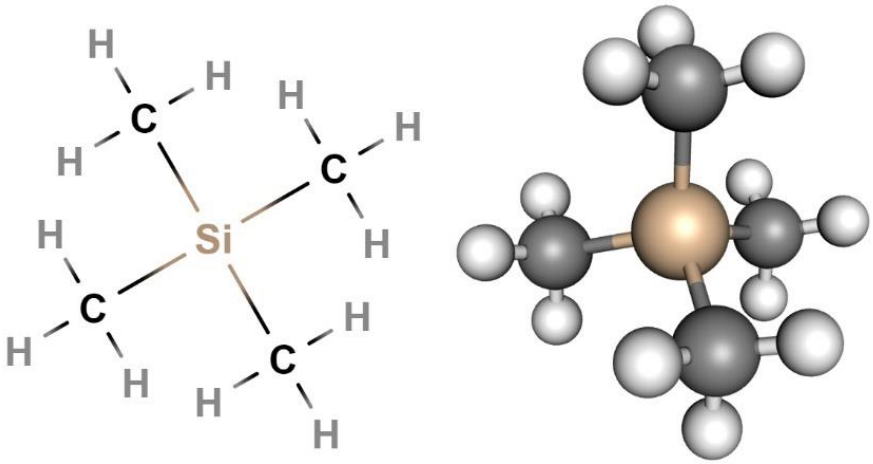


Figure 3. Tetramethylsilane precursor molecule structural formula image on the left and 3D ball and stick model on the right.

TMS is a nonpolar high vapor-pressure liquid having a boiling point of only 26 °C. For this reason, TMS needs to be stored in a refrigerator. To get a sample of TMS free from oxygen and avoid impurities in the resultant NCs, the TMS precursor was deoxygenated using a sparging technique. The TMS was sparged by bubbling nitrogen through the sample for 4 hours to remove other dissolved gases before being introduced into the synthesis reactor system. The TMS used in this study was purchased commercially at >99% purity. Figure 3 details the structure of TMS, which is tetrahedral at carbon and silicon.

TMS is commonly used in nuclear magnetic resonance spectroscopy as an internal standard for calibration due to the high symmetry of the compound: all twelve hydrogen atoms

are equivalent in TMS, so its proton spectrum is a very sharp singlet. This property of TMS drives consistent demand in the market, which drives down cost and makes it easily available to purchase online.

TMS has been used to make SiC NPs and thin films in prior research [26, 27, 38, 43, 44, 45]. As TMS has a carbon:silicon ratio of 4:1 in molecular form, prior literature reports logically indicate an excess of carbon in the final formed nanomaterial. Lin et al. reported tuning the carbon content of amorphous SiC NPs by adding hydrogen into the flow of a low pressure nonthermal plasma [26]. They directly measured the increase of waste methane gas coming out from their reactor and its correlation with added hydrogen by monitoring the gas using an online mass spectrometer. Hydrogen preferentially consumes the carbon content of the precursor while leaving the silicon ions to incorporate into the NPs. This even works in the silicon-rich case, to decrease the carbon content past 1:1 carbon:silicon. If the hydrogen atoms in the plasma could meet *all* the carbon ions in the plasma, carbon could in theory be removed entirely and pure silicon nanocrystals obtained. This has never been demonstrated in practice, however, probably due to the large amount of carbon present in TMS. Figure 4 shows a ternary plot of possible combinations of C-Si-H ratios in the plasma.

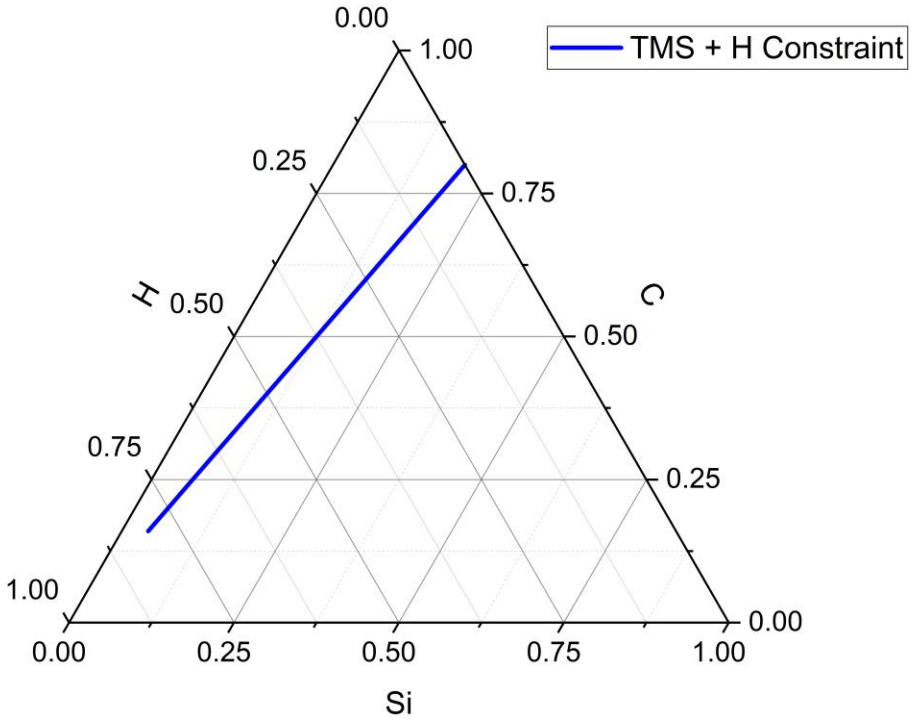


Figure 4. Ternary plot of possible combinations of composition ratios between silicon, carbon, and hydrogen. The blue line marks the only parameters that can be reached using TMS and hydrogen.

An expansion to the process would be to make SiC with dual precursors instead of with a single precursor containing both silicon and carbon atoms, such as TMS. This would be more materially efficient because instead of removing excess carbon, the ratio of silicon to carbon could be perfectly tuned and very little waste created. This tuning would allow the user to explore every possible ratio on Figure 4, giving more opportunities for what could be produced in the reactor. Liquid silicon precursors are safer than their smaller-molecule gaseous counterparts because they are less reactive with air [9, 46]. Additionally, other organosilicon compounds could be considered for a single precursor alongside TMS, including not only other alkylsilanes, but also silyl ethers, alkylsilenes, functionalized siloles, or even silatranes. Of course, with larger solid molecules comes the obstacle of sublimation.

# THE EXPERIMENTAL APPARATUS AND METHODOLOGY

Figure 5 displays the current plasma reactor setup at NDSU, which has gone through many iterations. The original apparatus which made silicon NCs was built by Todd Pringle and was expanded and adapted to make the SiC NCs described in this thesis [9].

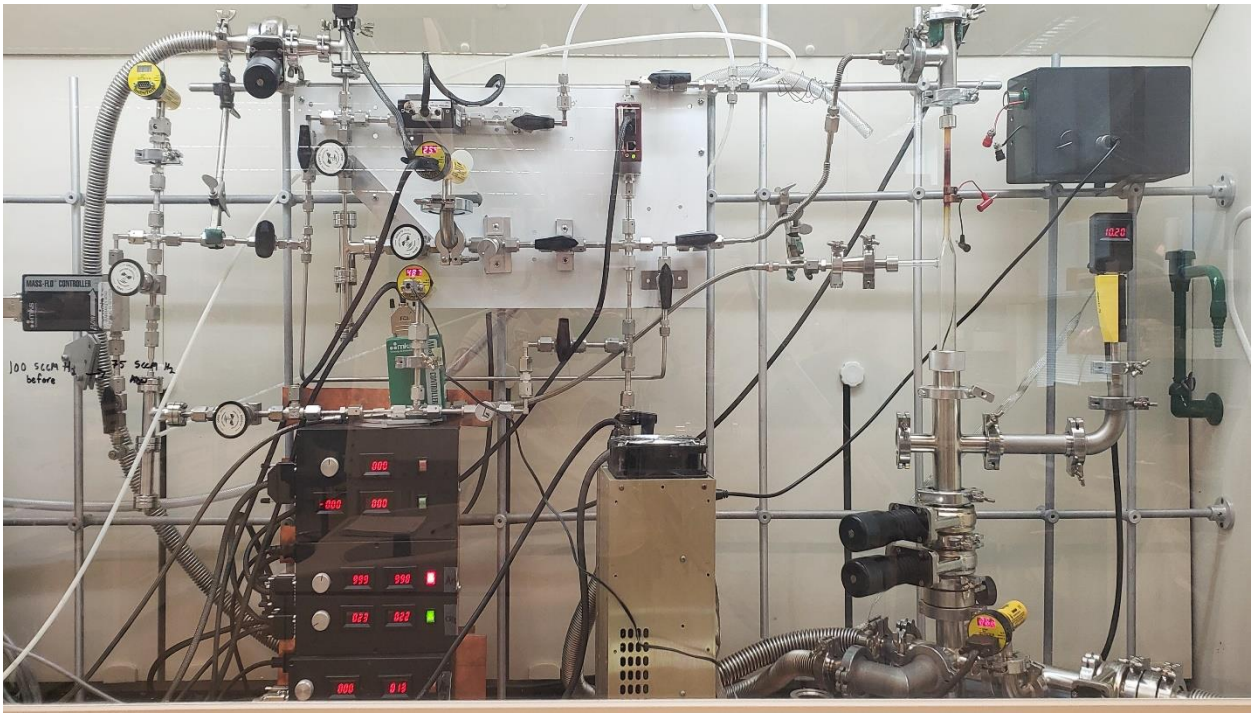


Figure 5. The expanded NDSU reactor with dual liquid precursor capabilities set up for hydrogen surface passivation of NCs. Setup was adjusted to for the hydrogen line to be plumbed for use as a reaction gas.

The basic working principle of the reactor is that a “precursor gas” is fed into a bubbler which contains the precursor. The precursor gas used as an input to the bubbler is a certified standard mixture of 95% argon/5% hydrogen and the precursor is TMS. An example of a liquid bubbler can be seen in Figure 6. The bubbler contains the liquid precursor, in which the input gas bubbles. A bubble starts at the bottom of the liquid, and as it rises TMS precursor molecules enter the bubble. At the interface of the liquid and the gaseous bubble, the TMS would be in equilibrium between the liquid and vapor states, with TMS as vapor entering the bubble. The

constant flow of gas into the bubbler pushes the precursor vapors downstream into the reactor. The bubbler was cooled in an ice bath down to near 0 °C during runs to further reduce the vapor pressure of the TMS, allowing for more control of the precursor flow rate. The flow rate of the precursor in a bubbler follows the next equation:

$$\frac{Q_{precursor}}{Q_{gas}} = \frac{P_{precursorVP}}{P_{bubbler} - P_{precursorVP}} \quad \text{(Eq. 2)}$$

where $Q_{precursor}$ is the precursor flow measured in SCCM, $Q_{gas}$ is the flow of the precursor gas, $P_{precursorVP}$ is the vapor pressure of the precursor measured in torr, and $P_{bubbler}$ is the pressure of the headspace of the bubbler.

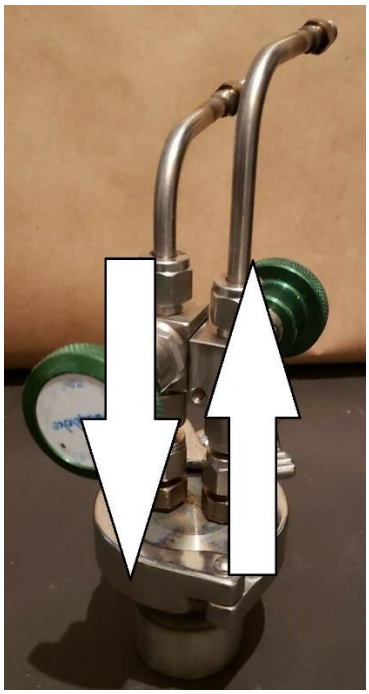

Figure 6. A liquid precursor bubbler. The arrows indicate the direction of gas flow. A long straw on the inlet side lowers down to the bottom of the liquid to bubble it.

Once the precursor gas leaves the bubbler, it joins up with a carrier gas. Carrier gas enables an operator to control the plasma characteristics, without requiring the full flow of gas to be directed through the liquid precursor. In our system, we use the same mixture of gas for

carrier gas as we use for the gas mixture used to generate the precursor vapor. Another gas used in this system is the reaction gas, which mediates the precursor in the plasma. In this system, hydrogen of 99.9995% purity (oxygen, water <1 ppm) is used as a reaction gas to control the amount of excess carbon in the final formed NCs. The vapor saturated precursor gas, carrier gas, and reaction gas all meet upstream of the reactor, and are introduced mixed into the plasma.

The carrier and reaction gases were controllably added to the reactor using mass flow controllers (MFCs). The MFCs were controlled using custom hardware, which created an analogue loop supplying up to 5 volts to the MFC and reading a 0-5 volt signal from the MFC to determine the actual amount of flow being released into the reactor. Flow rates are measured in standard cubic centimeters per minute (SCCM). The precursor and carrier gas MFCs were calibrated for argon. As we used a mixture of gases in the thermal-based MFCs, a gas correction factor was required. The equation for gas correction and its factors can be looked up on manufacturers' websites [47]:

$$Q = \frac{K_{used}}{K_{MFC}} Q_{readout} \qquad \text{(Eq. 3)}$$

where $Q$ is the amount of gas flowing through the MFC, $K_{used}$ is the gas correction factor of the gas flowing through the MFC, $K_{MFC}$ is the gas correction factor for the gas the MFC was calibrated for, and $Q_{readout}$ is the amount of flow that the MFC displays. The gas correction factor for hydrogen is 1.01 and for argon is 1.39. These values were determined by the manufacturers by using the gas densities and specific heats of the respective gases. Since our system uses a mixed gas, the gas flow constant for it can be found by weighting the gas correction factor by the ratio of gases; for a 95/5 mix of Ar/H, the gas correction factor is 1.37.

The plasma is driven by an RF power supply which has capability of going up to 300 watts of output power. The RF power is capacitively coupled to the plasma via two circular

copper strips (approximately 1 cm in width) which surround the reactor tube. The reactor tube varies based on the desired traits of the plasma, which generally follows Bernoulli's equation for flow through a pipe:

$$P_1 + \frac{1}{2}\rho v_1^2 + \rho g h_1 = P_2 + \frac{1}{2}\rho v_2^2 + \rho g h_2 \qquad \text{(Eq. 4)}$$

where $P$ is the pressure of the fluid, $\rho$ is the density of the fluid, $v$ is the velocity of the fluid, $g$ is the gravitational constant, and $h$ is the height of the fluid. Subscripts 1 and 2 denote the various system configurations that exist. For this system, we can neglect the third term on either side of the equation because the density of a gas is assumed to be small. This shows that for a larger diameter reactor tube, the gas flows slower through the pipe. Generally, to make homogeneous powders in this system and reduce reactor wall deposition, a larger diameter glass reactor was chosen. This reactor measured 0.69 inches in inner diameter, and 1 inch in outer diameter: the wall was about 0.16 inches thick. Such a thick wall allows for high plasma power to be used. The copper electrode connection area was actively cooled using compressed air to remove heat due to the high power used. The velocity of the gas can be found by equation 3-4:

$$v = \frac{Q_{T,P}}{A} = \frac{Q_{\mathrm{STP}}}{A}\,\frac{P_{\mathrm{STP}}T}{T_{\mathrm{STP}}P} = \frac{Q_{\mathrm{STP}}P_{\mathrm{STP}}}{A\,P} \qquad \text{(Eq. 5)}$$

which gives $v$, the velocity of the gas, in terms of $Q_{\mathrm{STP}}$, the flow of gas flowing through the MFC, $P$, the pressure read by the pressure transducers, $P_{\mathrm{STP}}$, which is equivalent to about 760 torr, and $A$, the cross-sectional area of the pipe. The final part of equation 3-4 implies a nonthermal plasma, that $T_{\mathrm{STP}} = T$. Using the velocity found in Eq. 3-4, the Reynolds number can be computed. For the 0.69 inch inner diameter tube, the flow is transitional between laminar and turbulent.

Between the RF power generator and electrodes is an impedance matching box. An impedance matching box minimizes the losses in the system by tuning the phase of the signal to find the optimum. Tuning must be considered because the signal is AC, and otherwise, large amounts of power will be wasted when converted to heat in either the power generator or the match box. Higher powers are required to reach power densities high enough to form SiC in a reactor this large, which is significantly larger than atmospheric pressure plasma reactors [27]. To counterbalance this, atmospheric pressure plasmas require higher power densities to sustain ionization compared to low-pressure plasmas, such as the one used in the NDSU reactor. To use concrete numbers, the power required to create SiC NCs is between 30-40 watts of net power (forward power less reflected power). However, higher powers up to 100 watts were useful in reacting more of the carbon precursor with hydrogen.

A two-stage mechanical vacuum pump was used to evacuate the reactor and maintain low pressures during the operation of the plasma. The vacuum pump was capable of pumping 21 cubic feet per minute and measured an ultimate pressure of <10 mtorr when exposed to the entire system. All low-pressure system parts were sealed with high-vacuum fittings, except the bubbler which is sealed with ultra-high-vacuum type fittings.

Connecting to the reactor, about 3 feet of 5-millimeter inner diameter tubing was used to deliver the input gases to the reactor. This resulted in turbulent flow (from the Reynolds number), mixing the gas-phase molecules upon entrance to the reactor, minimizing phase-rich pockets and engendering a uniform resultant powder. On the output of the reactor, a fine stainless-steel mesh was used to collect NPs: as the NPs are carried along in the gas, they strike the mesh and stick onto it. The mesh was placed between two gate valves, which allowed the powder to be brought into an oxygen-free glove box and keep the NCs completely unoxidized

when desired. The pressure of the reactor was moderated manually using a gate valve, and was kept constant for the run between 5 and 40 torr. The pressure at various points in the system was measured using a Pirani-type convection vacuum gauge, which is a gas-dependent gauge that had to be adjusted based on an estimate of the gas composition at that point in the system [48]. While reactor pressure is a vital parameter, remaining mindful of pressure changes across the entire system is helpful for process monitoring, control, and analysis.

During a synthesis reaction, typically 1 hour in length, a considerable amount of deposition forms on the reactor walls despite the plasma sheath discussed in the plasma theory section of the first chapter, the introduction. Most of the deposition in the synthesis process happens around the electrode locations, but some also happens downstream, where powder can be seen collecting lightly on the walls of the reactor, as in Figure 7. The electrode locations have thick deposition because of the neutral species in the plasma which are not repelled by the sheath. The plasma density is highest near the electrodes, which creates the high deposition concentration. The NC powder collects on the walls downstream of the plasma because there is no opposing force to stop it from doing so: the particles bump into the wall and no plasma sheath exists to repel the charged nanoparticles.

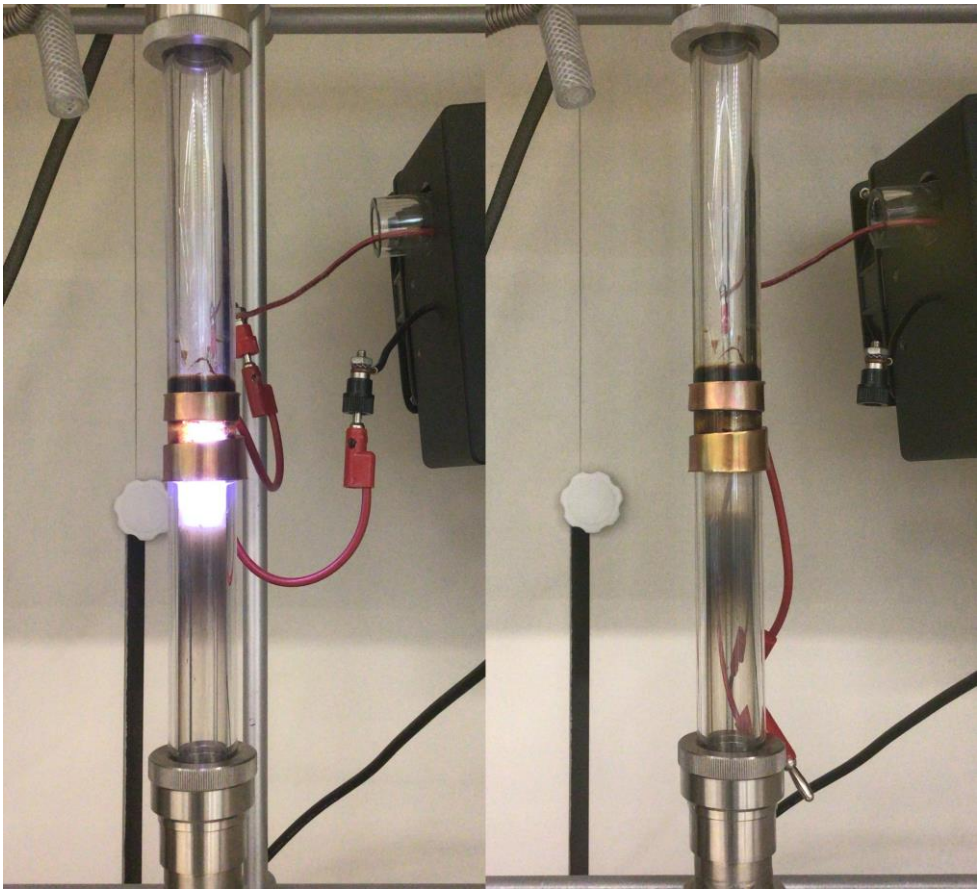

Figure 7. The synthesis reactor during and after a reaction. Near the electrodes is a thick film of deposited SiC, and downstream of the plasma can be seen a thin grey film of powder.

The particles deposited downstream of the reactor represent one of the largest yield losses in the system. It is largely unavoidable without a major overhaul to the system.

The characterizations performed on the powder were x-ray diffraction (XRD), thermogravimetric analysis (TGA), transmission electron microscopy (TEM), and optical absorption. The XRD data was collected on a Bruker D8 Discover diffractometer with a Cu K-α target. TGA was performed using a TA TGA Q500. TEM images were snapped on a JEOL JEM-2100 HRTEM. The sonicator used was a Cole-Parmer CPX130 20kHz system run at 40-70 forward watts commensurate with volume of solution.

# IN-SYSTEM NANOCRYSTAL TUNING

The system can be tuned in many different parameters. For the studies presented in this thesis, the precursor flow was kept constant, as was the size of the reactor, the distance of the electrodes, the powder collection method, and the plasma power (in that it was above the so-called “crystallization energy”). The tuning parameters chosen to vary were reactor pressure, reaction gas flow rate, and carrier gas flow rate. As can be inferred from Equation 3-4, an increase in flow of gas through the reactor will result in an increase of velocity through the reactor. A decrease in the pressure of the plasma, ceteris paribus, will also increase gas velocity though the plasma. The faster the gas moves through the plasma, the shorter the residence time. Thus, immediately, these tuning parameters should allow for size tuning of the nanoparticles.

The reaction gas allows for tuning the carbon content of the NCs, which tend to be either carbon-rich or silicon-rich. While the value of hydrogen gas does have an impact on the carbon content, the ratio of argon to carbon gas also has an impact on the overall carbon content. For example, in the scenario where 15 SCCM of hydrogen gas is used in conjunction with 80 SCCM of Ar:H 95/5 gas, the powder is carbon-rich, but if the Ar:H gas flow is reduced to 40 SCCM, the powder is silicon-rich, making a rich parameter space for tuning both size and Si:C elemental content.

Figure 8 displays some of the first powders made in the reactor. As a general trend, the powders became more homogeneous as the parameter space was mastered. The flakes in some of the pictures of powders in Figure 8 were the result of doing multiple runs in the same reactor without cleaning it. These flakes were avoided in characterization of the powder as the flakes were not consistent: the runs that composed the flakes would be difficult to reproduce in a

meaningful way. Despite this fact, the flakes could be potentially attractive as a future study because they exhibited white PL.

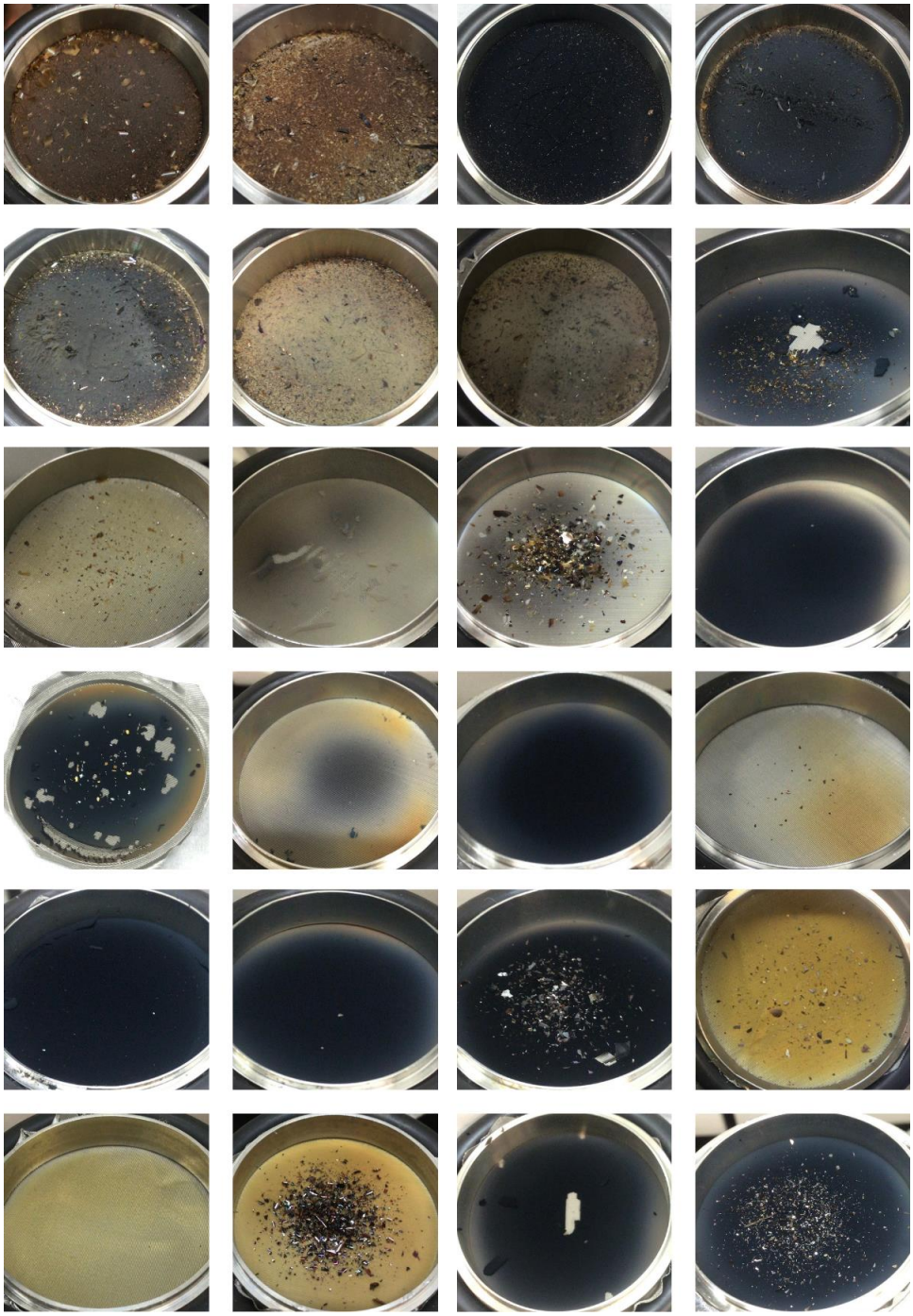

Figure 8. Images of some of the first successful syntheses of SiC NC powder ordered chronologically. Note the wide color variation hints at the composition of the powder.

The dark powdered samples in Figure 8 indicate an excess of carbon in the powder, while the lighter/yellow color indicates an excess of silicon in the powder. The yellow powder looks like silicon NC powder, which has a yellow-orange color [9]. This suggests that it has a similar absorption spectrum. This wide variation in color also demonstrates the change in optical and electronic properties of the material based on surface composition.

# RESULTS AND DISCUSSION

The results of this study focus on characterization of the SiC powder to understand its physical properties.

The yield of the powder was on par with other nonthermal plasma synthesis systems, on the milligram order of magnitude. A typical 1-hour run would allow for collection of 6 mg of powder, but would depend on how much hydrogen was used because the hydrogen consumes part of the precursor. The powder collects on the mesh wires, so its collection varies linearly with cross-sectional area covered by the mesh. Because the NPs collect on the mesh first and deposit upstream from there, gas flows between the NPs and the powder remains porous in an open fractal geometry.

Directly out of the synthesis system, the powder is expanded about 10 times from wetted aggregated packed spheres. To see it visually, a small amount of solvent, 10 µL, was added to a sampling of powder pictured in Figure 9. The powder goes into solution and dries in a much more densely packed form as the solvent evaporates.

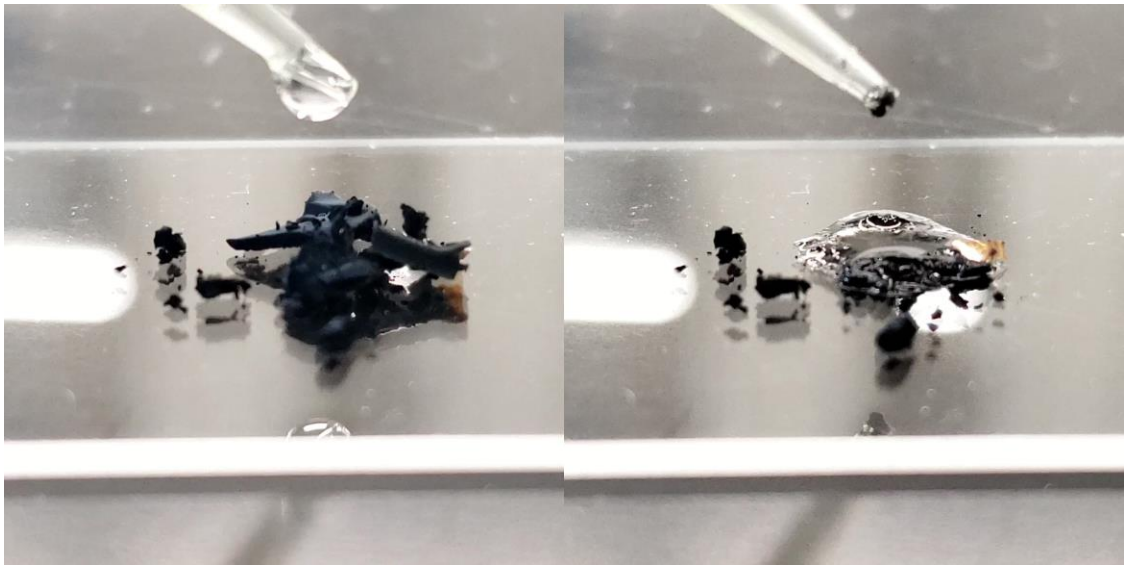

Figure 9. 1 mg of SiC NC powder wetted with 10 microliters of solvent.

**Solubility of nanocrystal powders and the surface**

The NCs went into solution in ethanol: as described in other papers, SiC NPs have intrinsic solubility in ethanol [25, 27, 39, 45]. The samples with large amounts of excess carbon would collect in the bottom of the vial if left to sit for adequate time, which depended on the particle size. To separate the particles from each other, the solutions were sonicated for 4 hours, and the particles that stayed in solution after being left for 8 hours stayed in solution indefinitely afterwards. The particles do not dissolve in water without some processing, but they do in alcohols, indicating that the particles require a medium polarity solvent (relative polarity 0.5 to 0.8); indeed, they also dissolve in methanol and isopropanol.

The solubility of the nanocrystals in alcohols strongly depends on how much excess amorphous carbon or excess silicon is present in the sample. Research on amorphous carbon coatings is significant and there are even some commercial products available that utilize the technology, such as scratch resistant thin films. Carbon as a shell has potentially useful properties due to the many bond hybridizations available to the carbon material system [49]. Despite its potential for functionalization, excess amorphous carbon on the surface has the potentially negative impact of decreasing the solubility of the SiC NCs in alcohol solvents. The samples were never found to be water soluble.

To remove the excess surface carbon, several methods could be employed. The two most common methods are acid-based removal and thermal oxidation. The acid-based removal route requires the use of concentrated nitric acid, a dangerous oxidizer. Due to this, thermally oxidizing the carbon away is the preferred method when access permits. We used a TGA to controllably oxidize the carbon at a constant temperature. Using the TGA also gives a quantitative measurement for how much carbon was removed from the powder. One sample

which had about 10% excess carbon was kept in the TGA for 5 hours at 500 °C to bake off the carbon. The data from the oxidation process is displayed in Figure 10.

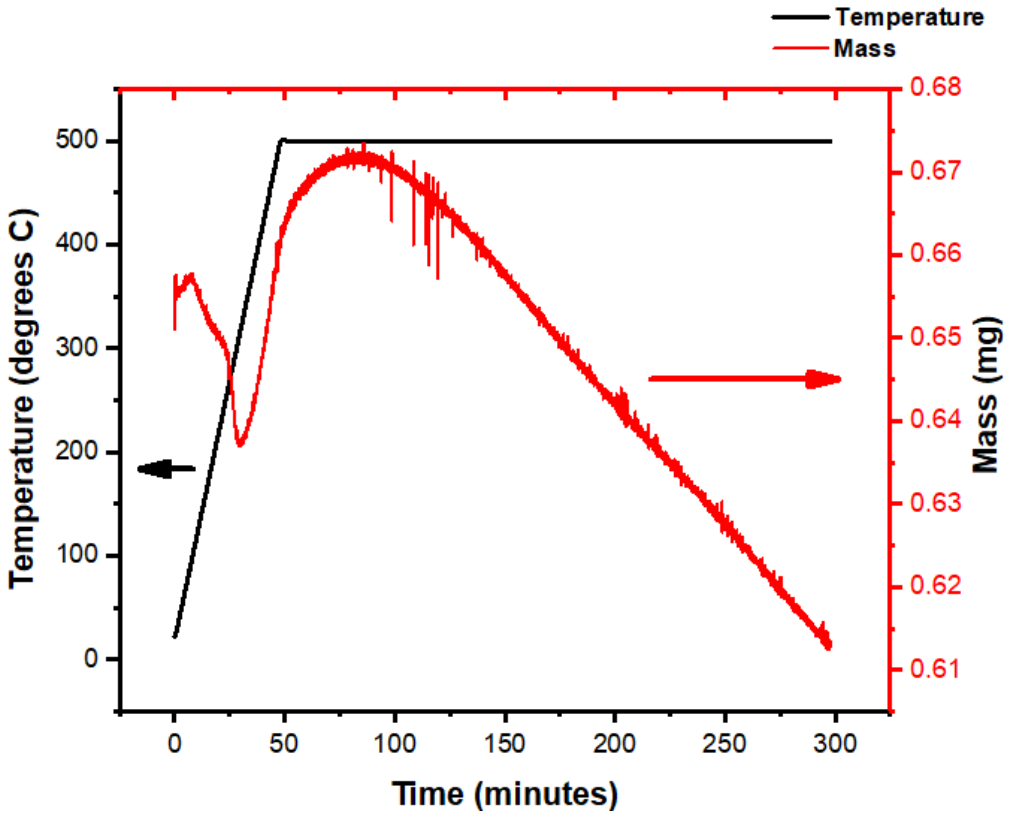


Figure 10. TGA data from a sample with about 10% excess carbon. The ramp to 500 °C burned off excess carbon material.

Figure 11 displays a TEM image of a sample SiC NCs with some of the most excess carbon on the surface. The amorphous shell can be seen around the lattice planes of individual particles and is up to 1 nm thick in the most extreme cases. As the natural ratio of carbon tends towards 4:1 due to the precursor, carbon excesses can be very high without the addition of hydrogen.

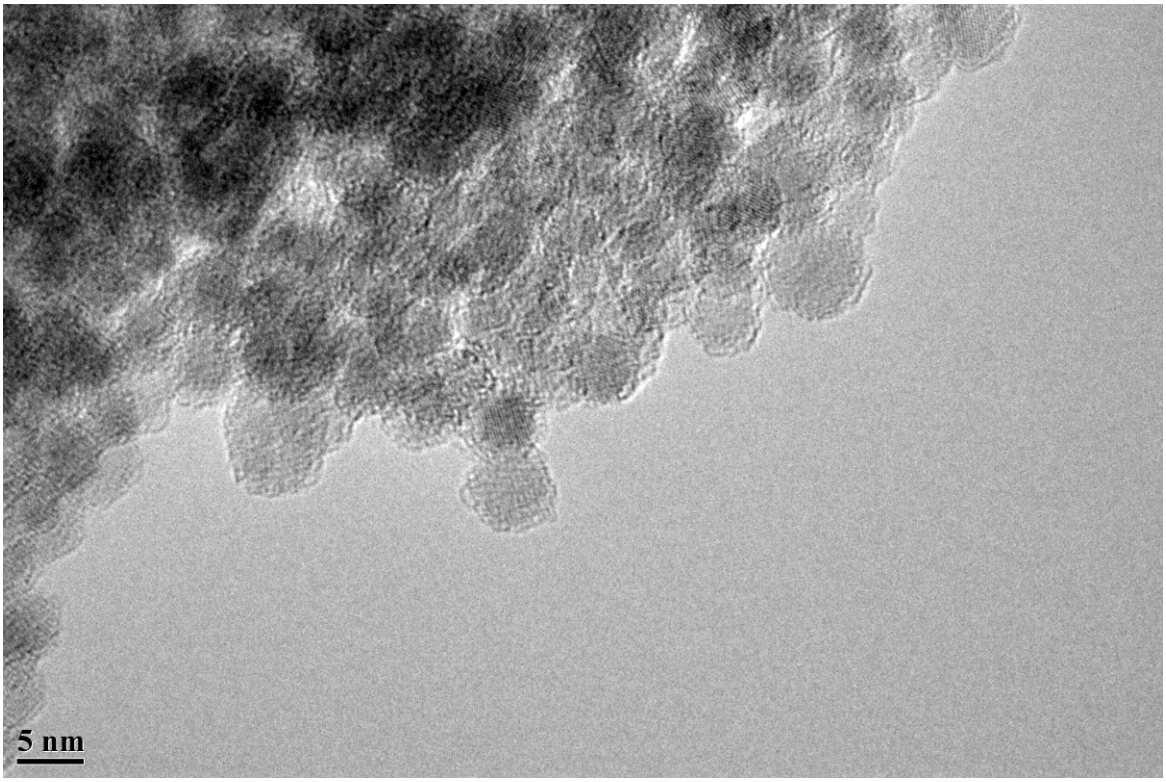


Figure 11. TEM image of SiC NC cores with amorphous carbon shells.

500 ° C is a temperature at which the carbon oxidizes but does not oxidize the silicon carbide. Over longer time scales, the SiC NCs may oxidize, as nanocrystalline SiC has been shown to undergo a diffusion mediated oxidization at temperatures as low as 783 °C for 200 nm sized particles [50]. The surface of SiC is known to oxidize at around 600 °C, and for increasingly smaller particles, the surface comprises more and more of the particle. Knowing this, we would expect our <5 nm sized particles to oxidize somewhere between 783 and 600 °C, though likely on the lower end of that range.

Figure 12 demonstrates the increased solubility of SiC NPs when the excess carbon is removed. The left vial contains an aliquot of unprocessed NCs sonicated in IPA for 4 hours. The right vial contains an aliquot of NCs after removing excess carbon and sonicating in IPA for 4 hours. This is the same sample as the data was taken in the TGA in Figure 10. The photograph shown in Figure 12 was taken after the two solutions had been left sedentary for several hours. It

is clear to see the aliquot with excess carbon has aggregated and settled to the bottom of the vial, while the aliquot without as much excess carbon stayed in a uniform solution in IPA.

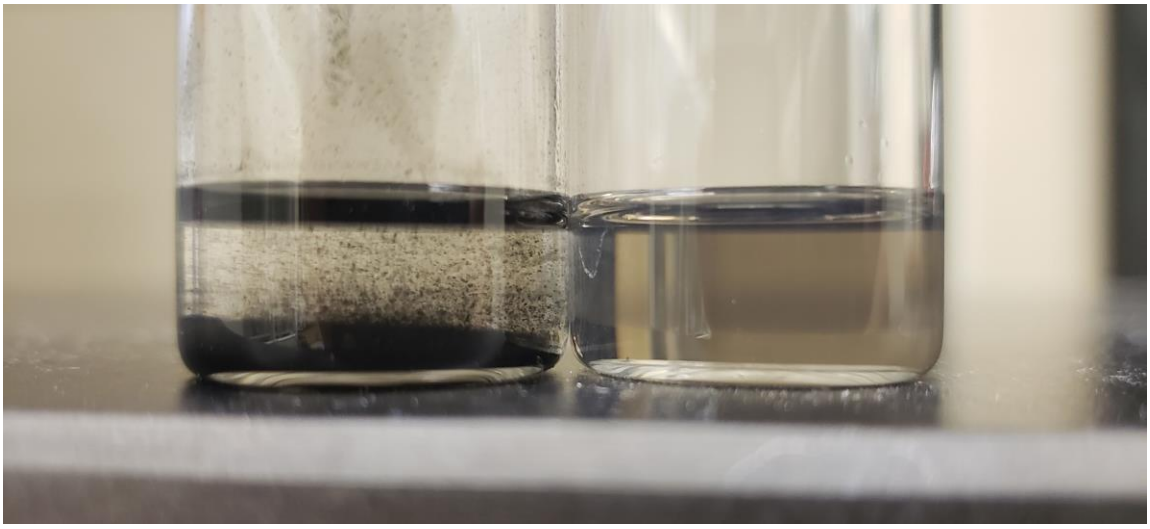

Figure 12. Solubility of silicon nanoparticles is greatly enhanced upon removal of excess carbon. The left is before and the right is after being processed in the TGA.

**Size variation, morphology, and identification of nanocrystal powder**

The individual particles can be viewed with an electron microscope, and the size and morphology can be directly seen. The particles were spherical and formed in sizes from 1.5 nm to 4.5 nm in diameter, depending on reactor conditions. The main parameter of the synthesis system used to vary size was the carrier gas flow rate because it is the least intertwined variable. The smallest particles were achieved with high flow rates. Figure 13 displays some typical TEM images taken of the particles. From the zoomed-in view, the individual lattice planes of the particles can be seen.

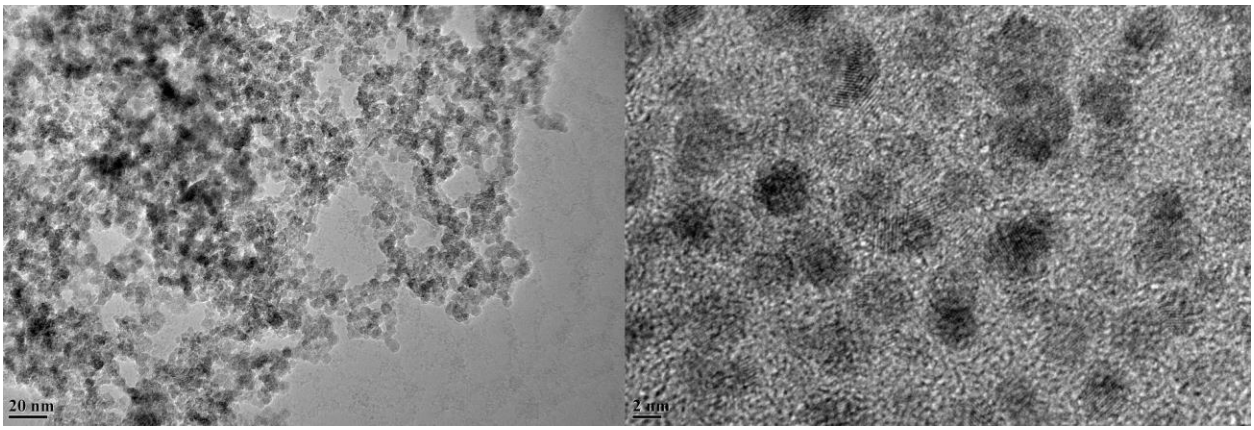


Figure 13. Two HRTEM images of SiC NCs. The left image is a birds-eye view of particles directly harvested from the mesh, the right image displays individual NCs.

From TEM images, we measure both the particle size (by measuring the diameter of the particles directly) and the lattice spacing of the particles, to confirm that the powder is indeed SiC and to determine which polymorph of SiC we have. TEM analysis of our samples has consistently revealed lattice spacings close to 0.25 nm, which can be indexed to the (111) plane of 3C-SiC with a cubic unit cell parameter of 0.436 nm [51]. This observation is consistent with the universal experimental findings that the cubic crystal structure of SiC is more probable than the hexagonal structure for small (<5 nm) NCs.

Figure 14 shows the TEM analysis technique. The yellow ring displays a size measurement of a NC. The inset graph shows the grey intensity of a line drawn through the nanocrystal perpendicularly to the lattice planes and averaged across 20 pixels. A brief calculation of the example in Figure 14 shows that the average lattice spacing for this NC is $\frac{3.5\ nm}{14}$ = 0.25 nm, which is the expected dominant (111) lattice spacing for 3C-SiC.

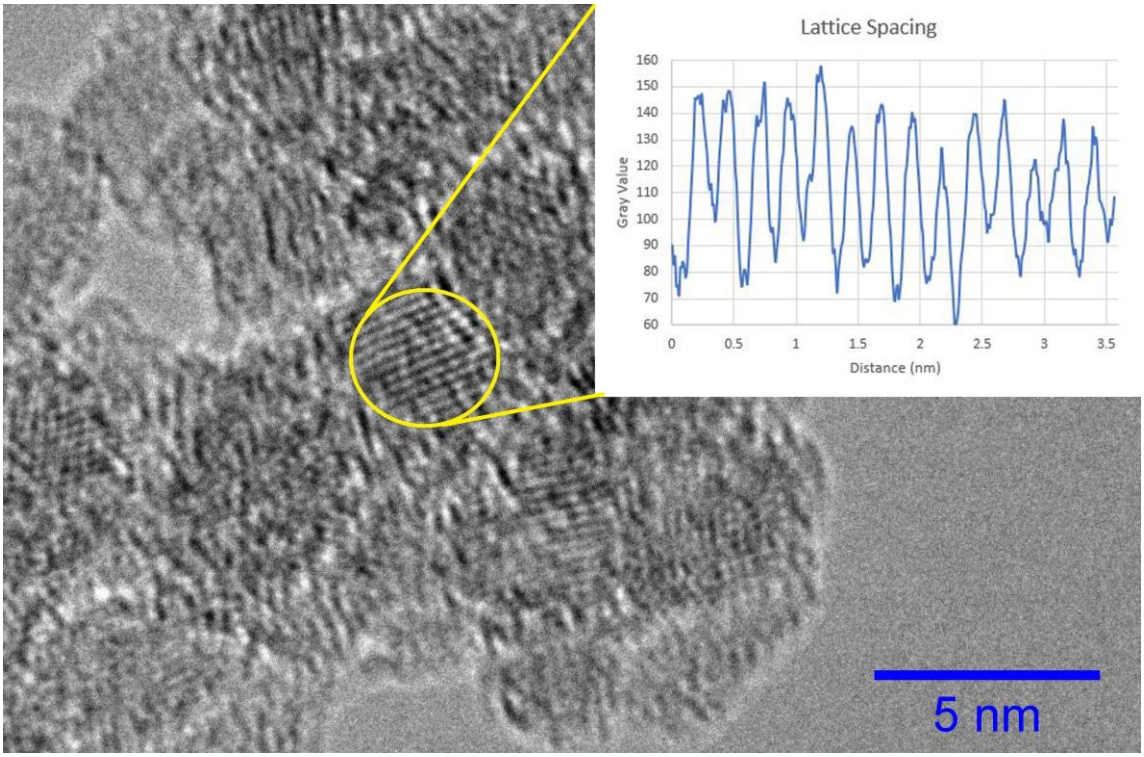


Figure 14. TEM analysis of individual SiC crystals for size and lattice spacing.

Further confirmation of the 3C-SiC structure of the powder is found using XRD. XRD can also be used to find the size of the ordered crystalline domains through the Scherrer equation

$$\tau = \frac{K\lambda}{\beta \cos(\theta)} \qquad \text{(Eq. 6)}$$

where $\tau$ is the mean size of the ordered domains, $K$ is the shape factor (taken to be 0.94 for spherical crystals with cubic symmetry), $\lambda$ is the x-ray wavelength, $\beta$ is the line broadening at half the maximum intensity, and $\theta$ is the Bragg angle. Due to the Scherrer-derived sizing being dependent upon crystal domain size, it is helpful to keep in mind that the actual size of the particles may be larger, depending upon how much amorphous carbon coats the outside of the NCs.

Figure 15 displays the XRD data taken for Scherrer-derived sizes of 4.12 nm, 3.46 nm, and 2.87 nm particles, all showing strong line broadening. The (111) peak is the strongest, which

agrees with the TEM measurements and is easily visible. The (220) and (311) peaks were comparatively weaker, and all three lined up with expected diffraction peaks for the beta polymorph of SiC.

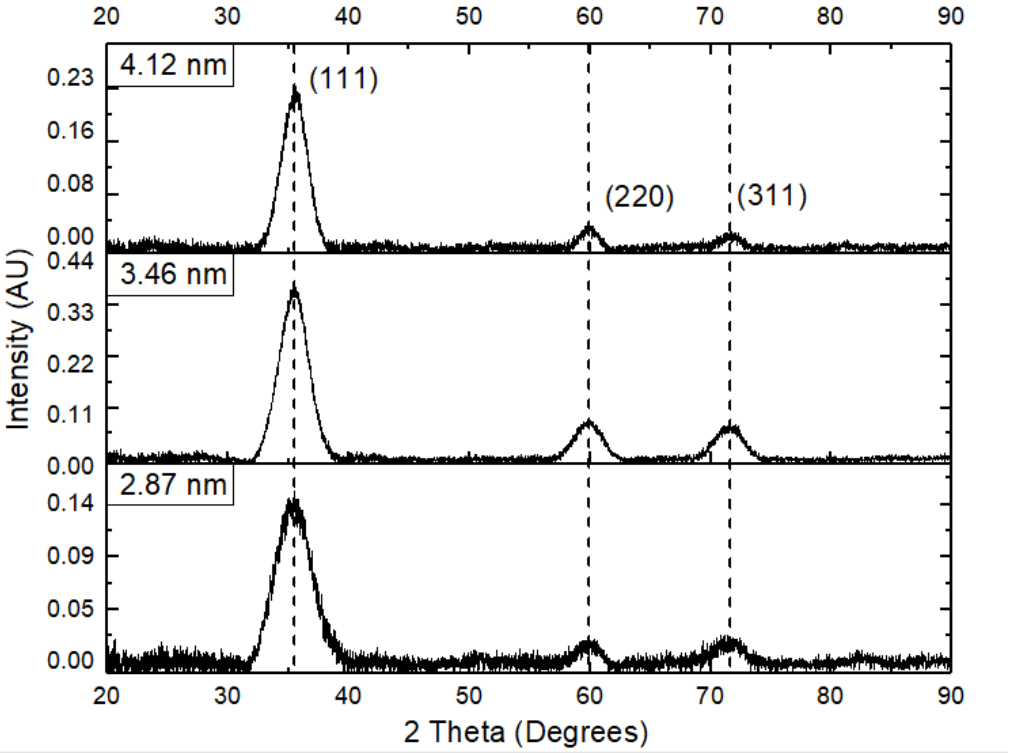


Figure 15. X-Ray diffraction data for silicon carbide with the lines indexed to the (111), (220), and (311) planes of the beta polymorph for three different sizes of nanocrystals.

**Optical absorption**

Optical absorption of the powder was performed by placing a small amount of carbon-removed powder in an IPA solution. Concentrations were low, on the order of 0.1 mg/mL. The carbon had to be removed first such that the amorphous carbon coating would not interfere with the signal and an approximate band gap value could be determined through what is commonly referred to as a Tauc plot. The Tauc plot shows the photon energy on the abscissa and the quantity $(\alpha h\nu)^{0.5}$ on the ordinate, where $\alpha$ is the absorption coefficient and $h\nu$ represents the

photon energy. The exponent denotes the nature of the band gap transition, and a factor of 0.5 denotes an indirect allowed transition.

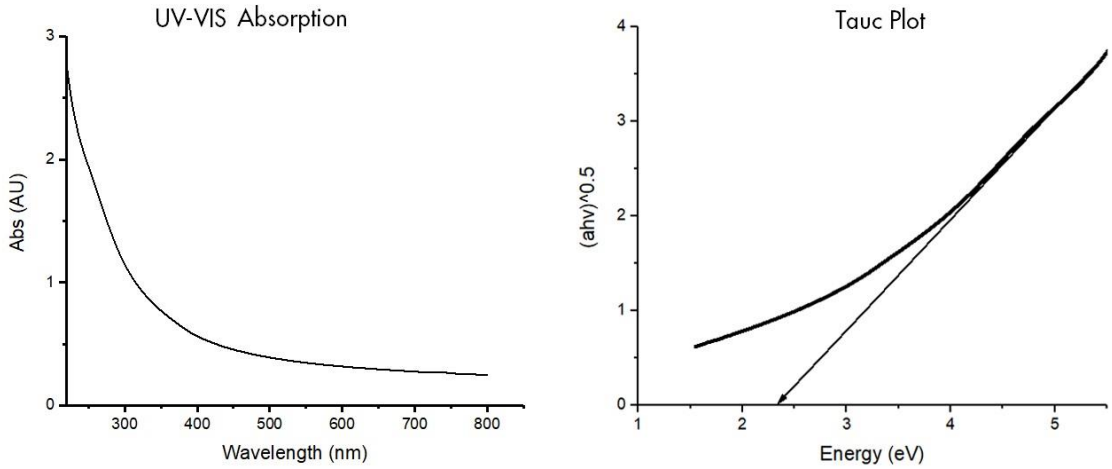


Figure 16. The left figure represents the UV-Visible absorption plot of silicon carbide nanocrystals. The right figure represents the associated Tauc plot, and when extrapolated to the abscissa shows a band gap of just under 2.4 eV.

The linear region of Figure 16 extrapolates the optical absorption spectrum to the abscissa, denoting the approximate optical band gap of the material, which is just under 2.4 eV. This agrees well with the generally accepted bulk band gap of 3C-SiC, 2.36 eV. Baseline measurements were subtracted to negate the absorption of the IPA solvent.

**Increasing yields**

Taking advantage of the dual precursor capabilities of the NDSU reactor, a few runs were tried with added cyclohexasilane precursor (a pure silicon source) “mixed” with the TMS precursor. Without hydrogen, this still resulted in a carbon-rich product. However, it had a noticeably higher yield, filling the mesh in ¼ of the time. Adding cyclohexasilane allows the user to explore the space below the TMS - H line of Figure 4. This thesis does not explore this parameter space because it changes the composition of the material. Not only that, the differing dissociation energies of the two molecules would create silicon- or carbon-rich pockets in the plasma which changes the morphology of the nanoparticles, introducing yet another variable in

an already complex system. In the end, increasing yields is the most significant challenge to bringing this ultra-pure form of nanocrystalline silicon carbide to market.

# CONCLUSION AND OUTLOOK

Nanoparticles have diverse and interesting properties due to their small size. These distinct properties enable technological advancements in practical applications such as LEDs and photovoltaic cells, biosensing and imaging, water treatment, novel coatings, and more. Until now, synthesis of small silicon carbide (<5 nm) nanocrystals was not well understood. Their properties are conflicting in the literature: some have photoluminescence while others do not, and some are water soluble while others are not.

In this study, beta polymorph small silicon carbide nanocrystals were made in a low pressure nonthermal plasma reactor. Silicon carbide nanocrystals of this size have never been made with this method before. The radii of the nanocrystal spheres were varied by changing the reactor pressure and precursor flow rates through the reactor, and the sizes were confirmed by both XRD and TEM measurements. The tetramethylsilane precursor has excess carbon that was consumed by hydrogen in the plasma, engendering a stoichiometrically balanced end result. If the exact amount of hydrogen was not added to the unbalanced precursor, the powder ended up either carbon- or silicon-rich, which formed an amorphous shell around the particles. The carbon-rich nanocrystals were soluble in short-chain alcohols and the silicon-rich nanocrystals were not. The optical band gap of the nanocrystals was 2.4 eV, the same as the bulk polymorph. Beta silicon carbide is useful for its extreme hardness, with 95% of the hardness of diamond and its robust semiconductor properties.

Future work could include more precursors. Phenylsilane groups, diethylsilane, di-tert-butylsilane, hexylsilane, and diethylsilane are all potential candidates as a dual-molecule precursor for silicon carbide. Each molecule has unique dissociation characteristics, which will change how and where it vaporizes in the plasma. Although silicon precursor was added to the

tetramethylsilane to increase yield in our study, dual precursors with direct silicon and carbon molecules would allow for further tuning the Si:C ratio and more efficient use of precursors through increased yield: carbon would not need to be consumed by the hydrogen gas, reducing loss.

In the future, further functionalization and ligation studies could be pursued. If a clean surface of SiC or Si-rich material is present, the hydrogen passivated silicon atoms could undergo hydrosilylation where an alkene or alkyne bonds with the surface silicon atoms on the double or triple bond site [52, 53]. This would give it more solution properties similar to silicon nanocrystals, which have been studied extensively. Likewise, the carbon-rich shell surrounding the particles could be functionalized to make them react differently to their environment. Additionally, photoluminescence could be another avenue to explore. Devices using the nanocrystals could show future potential due to silicon carbide's distinct inertness and stability, especially when compared to unstable perovskites or even silicon.

The powder collected from the reactor could also be experimented on further. Since the powder matrix is so porous, sintering and filling the matrix with other materials such as polymers or other semiconductors could yield physically robust, functional nanomaterial composites.

In summary, silicon carbide is an inert substance which requires high synthesis temperatures. We made small silicon carbide nanocrystals without heating bulk amounts of material via energetic surface reactions in a nonthermal plasma. We collected crystals with sizes between 1.5 and 4.5 nm, with both silicon-rich and carbon-rich shells. The amorphous carbon shells were removed by thermal oxidation which increased particle solubility in alcohols.

# REFERENCES


[1] J. F. Shackelford, S.-H. Kwon, S. Kim and Y.-H. Han, CRC Materials Science and Engineering Handbook, fourth ed., Boca Raton, Florida: CRC Press, 2016.

[2] R. P. Devaty and W. J. Choyke, "Optical characterization of silicon carbide polytypes," *physica status solidi (a)*, vol. 1, no. 162, pp. 5-38, 1997.

[3] M. D. P. Emilio, "Silicon Carbide for the Success of Electric Vehicles," Power Electronics News, 3 August 2020. [Online]. Available: https://www.powerelectronicsnews.com/silicon-carbide-for-the-success-of-electric-vehicles/. [Accessed 24 January 2021].

[4] G. Calusine, A. Politi and D. D. Awschalom, "Silicon carbide photonic crystal cavities with integrated color centers," *Applied Physics Letters*, 2014.

[5] R. Brook, M. Bever and R. Cahn, Concise encyclopedia of advanced ceramic materials, Pergamon Press, 1991.

[6] ISO, "19749," in *Nanotechnologies - Measurements Of Particle Size And Shape Distributions By Scanning Electron Microscopy*, Geneva, Switzerland, International Organization for Standardization, 2020.

[7] ASTM, "E3247 - 20," in *Standard Test Method for Measuring the Size of Nanoparticles in Aqueous Media Using Dynamic Light Scattering*, West Conshohocken, American Society for Testing and Materials, 2020.

[8] C. B. Murray, D. J. Norris and M. G. Bawendi, "Synthesis and Characterization of Nearly Monodisperse CdE (E = S, Se, Te) Semiconductor Nanocrystallites," *Journal of the American Chemical Society*, vol. 9, no. 115, pp. 8706-8715, 1993.

[9] T. A. Pringle, K. I. Hunter, A. Brumberg, K. J. Anderson, J. A. Fagan, S. A. Thomas, R. J. Petersen, M. Sefannaser, Y. Han, S. L. Brown, D. S. Kilin, R. D. Schaller, U. R. Kortshagen, P. R. Boudjouk and E. K. Hobbie, "Bright Silicon Nanocrystals from a Liquid Precursor: Quasi-Direct Recombination with High Quantum Yield," *ACS Nano,* vol. 14, pp. 3858-3867, 2020.

[10] A. Veamatahau, B. Jiang, T. Seifert, S. Makuta, K. Latham, M. Kanehara, T. Teranishi and Y. Tachibana, "Origin of surface trap states in CdS quantum dots: relationship between size dependent photoluminescence and sulfur vacancy trap states," *Physical Chemistry Chemical Physics,* vol. 17, pp. 2850-2858, 2015.

[11] L. Wang, Q. Cheng, H. Qin, Z. Li, Z. Lou, J. Lu, J. Zhang and Q. Zhou, "Synthesis of silicon carbide nanocrystals from waste polytetrafluoroethylene," *Dalton Transactions,* no. 46, pp. 2756-2759, 2017.

[12] Z.-F. Zhang, Y. Mu, F. Babonneau, R. M. Laine, J. F. Harrod and J. A. Rahn, Polymethylsilane as a Precursor to High Purity Silicon Carbide. In: Harrod J.F., Laine R.M. (eds) Inorganic and Organometallic Oligomers and Polymers, Springer, 1991.

[13] A. A. Zhokhov, V. M. Masalov, D. V. Matveev and M. Y. Maksumik, "II Zver kova, SS Khasanov, SZ Shmurak, AP Bazhenov and GA Emel chenko.," *Phys. Sol. State,* no. 51, p. 1626, 2009.

[14] A. Parvizi-Majidi, Comprehensive Composite Materials: Fiber Reinforcements and General Theory of Composites, Elsevier, 2000.

[15] J. S. Shor, X. G. Zhang and R. M. Osgood, "Laser-assisted photoelectrochemical etching of n-type beta-SiC," *Journal of The Electrochemical Society,* vol. 4, no. 139, p. 1213, 1992.

[16] X. L. Wu, J. Y. Fan, T. Qiu, X. Yang, G. G. Siu and P. K. Chu, "Experimental evidence for the quantum confinement effect in 3 C-SiC nanocrystallites," *Physical Review Letters,* vol. 2, no. 94, p. 026102, 2005.

[17] J. Botsoa, J. M. Bluet, V. Lysenko, O. Marty, D. Barbier and G. Guillot, "Photoluminescence of 6H–SiC nanostructures fabricated by electrochemical etching," *Journal of Applied Physics,* vol. 102, no. 8, 2007.

[18] E. J. Henderson and J. G. C. Veinot, "From Phenylsiloxane Polymer Composition to Size-Controlled Silicon Carbide Nanocrystals," *Journal of the American Chemical Society,* vol. 131, no. 2, pp. 809-815, 2009.

[19] E. P. Simonenko, N. P. Simonenko, A. V. Derbenev, V. A. Nikolaev, D. V. Grashchenkov, V. G. Sevastyanov, E. N. Kablov and N. T. Kuznetsov, "Synthesis of Nanocrystalline Silicon Carbide Using the Sol-Gel Technique," *Russian Journal of Inorganic Chemistry,* vol. 58, no. 10, pp. 1143-1151, 2013.

[20] S. T. Aruna and A. S. Mukasyan, "Combustion synthesis and nanomaterials," *Current opinion in solid state and materials science,* vol. 12, no. 3-4, pp. 44-50, 2008.

[21] J. Boucle, N. Herlin-Boime and A. Kassiba, "Influence of silicon and carbon excesses on the aqueous dispersion of SiC nanocrystals for optical application," *Journal of Nanoparticle Research,* vol. 7, no. 2, pp. 275-285, 2005.

[22] N. Rao, B. Micheel, D. Hansen, C. Fandrey, M. Bench, S. Girshick, J. Heberlein and P. McMurry, "Synthesis of nanophase silicon, carbon, and silicon carbide powders uning a plasma expansion process," *Journal of Materials Research*, vol. 10, no. 8, pp. 2073-2084, 1995.

[23] D. Coleman, T. Lopez, O. Yasar-Inceoglu and L. Mangolini, "Hollow silicon carbide nanoparticles from a non-thermal plasma process," *Journal of Applied Physics*, vol. 117, no. 19, p. 193301, 2015.

[24] F. Vivet, A. Bouchoule and L. Boufendi, "Synthesis and characterization of SiC: H ultrafine powder generated in an argon–silane–methane low-pressure radio-frequency discharge," *Journal of Applied Physics*, vol. 83, no. 12, pp. 7474-7481, 1998.

[25] G. Viera, J. Costa, P. Roura and E. Bertran, " High nucleation rate in pure SiC nanometric powder by a combination of room temperature plasmas and post-thermal treatments," *Diamond and Related Materials*, vol. 8, no. 2-5, pp. 364-368, 1999.

[26] H. Lin, J. A. Gerbec, M. Sushchikh and E. W. McFarland, "Synthesis of amorphous silicon carbide nanoparticles in a low temperature low pressure plasma reactor," *Nanotechnology*, vol. 19, no. 32, p. 325601, 2008.

[27] S. Askari, A. U. Haq, M. Macias-Montero, I. Levchenko, F. Yu, W. Zhou, K. K. Ostrikov, P. Manguire, V. Svrcek and D. Mariotti, "Ultra-small photoluminescent silicon-carbide nanocrystals by atmospheric-pressure plasmas," *Nanoscale*, vol. 8, no. 39, pp. 17141-17149, 2016.

[28] U. F. &. D. Administration, "Mercury Vapor Lamps (Mercury Vapor Light Bulbs)," 28 September 2020. [Online]. Available: https://www.fda.gov/radiation-emitting-products/home-business-and-entertainment-products/mercury-vapor-lamps-mercury-vapor-light-bulbs#d. [Accessed 30 January 2021].

[29] U. R. Kortshagen, R. M. Sankaran, R. N. Pereira, S. L. Girshick, J. J. Wu and E. S. Aydil, "Nonthermal Plasma Synthesis of Nanocrystals: Fundamental Principles, Materials, and Applications," *ACS Chemical Reviews,* vol. 116, pp. 11061-11127, 2016.

[30] L. Mangolini and U. R. Kortshagen, "Selective nanoparticle heating: Another form of nonequilibrium in dusty plasmas," *Physical Review E,* vol. 79, no. 2, p. 026405, 2009.

[31] D. Thiry, S. Konstantinidis, J. Cornil and R. Snyders, "Plasma diagnostics for the low-pressure plasma polymerization process: A critical review," *Thin Solid Films,* vol. 606, no. 1, pp. 19-44, 2016.

[32] P. Chambert and N. Braithwaite, Physics of Radio Frequency Plasmas, Cambridge: Cambridge University Press, 2011.

[33] R. Yakimova, R. M. Petoral Jr, G. R. Yadzi, C. Vahlberg, A. L. Spetz and K. Uvdal, "Surface functionalization and biomedical applications based on SiC," *Journal of Physics D: Applied Physics,* vol. 40, no. 20, p. 6435, 2007.

[34] J. Fan, H. Li, J. Jiang, L. So, Y. W. Lam and P. Chu, "3C–SiC Nanocrystals as Fluorescent Biological Labels," *Small,* vol. 4, no. 8, pp. 1058-1062, 2008.

[35] K.-Y. Cheng, R. Anthony, U. R. Kortshagen and R. J. Holmes, "High-efficiency silicon nanocrystal light-emitting devices," *Nano Letters,* vol. 11, no. 5, pp. 1952-1956, 2011.

[36] S. Niesar, W. Fabian, N. Petermann, D. Herrmann, E. Riedle, H. Wiggers, M. S. Brandt and M. Stutzmann, "Efficiency enhancement in hybrid P3HT/silicon nanocrystal solar cells," *Green*, vol. 1, no. 5-6, pp. 339-350, 2011.

[37] F. Meinardi, S. Ehrenberg, L. Dhamo, F. Carulli, M. Mauri, F. Bruni, R. Simonutti, U. R. Kortshagen and S. Brovelli, "Highly efficient luminescent solar concentrators based on earth-abundant indirect-bandgap silicon quantum dots," *Nature Photonics*, vol. 11, no. 3, pp. 177-185, 2017.

[38] A. U. Haq, M. Buerkle, S. Askari, C. Rocks, C. Ni, V. Švrček, P. Maguire, J. T. Irvine and D. Mariotti, "Controlling the Energy-Level Alignment of Silicon Carbide Nanocrystals by Combining Surface Chemistry with Quantum Confinement," *The Journal of Physical Chemistry Letters*, vol. 11, no. 5, pp. 1721-1727, 2020.

[39] D. Beke, Z. Szekrényes, Z. Czigány, K. Kamarás and Á. Gali, "Dominant luminescence is not due to quantum confinement in molecular-sized silicon carbide nanocrystals," *Nanoscale*, vol. 7, no. 25, pp. 10982-10988, 2015.

[40] A. M. Rossi, T. E. Murphy and V. Reipa, "Ultraviolet photoluminescence from 6 H silicon carbide nanoparticles," *Applied Physics Letters*, vol. 92, no. 25, p. 253112, 2008.

[41] J. Fan, H. Li, J. Wang and M. Xiao, "Fabrication and photoluminescence of SiC quantum dots stemming from 3C, 6H, and 4H polytypes of bulk SiC," *Applied Physics Letters*, vol. 101, no. 13, p. 131906, 2012.

[42] X. Guo, Y. Zhang, B. Fan and J. Fan, "Quantum confinement effect in 6H-SiC quantum dots observed via plasmon–exciton coupling-induced defect-luminescence quenching," *Applied Physics Letters*, vol. 110, no. 12, p. 123104, 2017.

[43] N. Herlin, M. Lefebvre, M. Pealat and J. Perrin, "Investigation of the chemical vapor deposition of silicon carbide from tetramethylsilane by in situ temperature and gas composition measurements," *The Journal of Physical Chemistry,* vol. 96, no. 17, pp. 7063-7072, 1992.

[44] W. Zhang, M. Lelogeais and M. Ducarroir, "Process study of silicon carbide coatings deposited on steel by plasma-assisted chemical vapor deposition from tetramethylsilane-argon gas system," *Japanese Journal of Applied Physics,* vol. 31, no. 12R, p. 4053, 1992.

[45] A. U. Haq, P. Lucke, J. Benedikt, P. Maguire and D. Mariotti, "Dissociation of tetramethylsilane for the growth of SiC nanocrystals by atmospheric pressure microplasma," *Plasma Processes and Polymers,* vol. 17, no. 5, p. 1900243, 2020.

[46] E. Wiberg, "Alfred Stock and the Renaissance of Inorganic Chemistry," *Pure and Applied Chemistry,* vol. 49, pp. 691-700, 1977.

[47] M. Instruments, "Gas Correction Factors for Themal-Based Mas Flow Controllers," 2018. [Online]. Available: https://www.mksinst.com/n/gas-correction-factors-for-thermal-based-mass-flow-controllers. [Accessed 8 1 2021].

[48] K. Jousten, "On the gas species dependence of Pirani vacuum gauges," *Journal of Vacuum Science & Technology A: Vacuum, Surfaces,* vol. 26, no. 3, pp. 352-359, 2008.

[49] R. P. Silva, Properties of Amorphous Carbon, INSPEC, 2003.

[50] J. Quanli, Z. Haijun, L. Suping and J. Xiaolin, "Effect of particle size on oxidation of silicon carbide powders," *Ceramics International,* no. 33, pp. 309-3133, 2007.

[51] R. J. Iwanowski, K. Fronc, W. Paszkowicz and M. Heinonen, "XPS and XRD study of crystalline 3C-SiC grown by sublimation method," *Journal of Alloys and Compounds,* vol. 286, no. 1-2, pp. 143-147, 1999.

[52] S. Alekseev, E. Shamatulskaya, M. Volvach, S. Gryn, D. Korytko, I. Bezverkhyy, V. Iablokov and V. Lysenko, "Size and Surface Chemistry Tuning of Silicon Carbide Nanoparticles," *Langmuir*, vol. 33, pp. 13561-13571, 2017.

[53] M. Rosso, A. Arafat, K. Schroën, M. Giesbers, C. S. Roper, R. Maboudian, and H. Zuilhof, "Covalent attachment of organic monolayers to silicon carbide surfaces," *Langmuir*, vol. 24, no. 8, pp. 4007-4012, 2008.

[54] N. Rao, N. Tymiak, J. Blum, A. Neuman, H. Lee, S. Girshick, P. McMurry and J. Heberlein, "Hypersonic plasma particle deposition of nanostructured silicon and silicon carbide," *Journal of Aerosol Science,* vol. 29, no. 5-6, pp. 707-720, 1998.